CONF-890855--19

CONF-890855--19

DE89 010259

RADIATION EMBRITTLEMENT OF PWR VESSEL SUPPORTS

R. D. Cheverton G. C. Robinson
W. E. Pennell R. K. Nanstad

Oak Ridge National Laboratory
P.O. Box 2009
Oak Ridge, Tennessee 37831-8056

Early in 1978 it became apparent that the fast neutron spectrum above 0.1 MeV was much softer in the PWR cavity than in the MTRs. Because of this, and because neutrons with energies in the range of 0.1 to 1.0 MeV contribute to radiation damage, correlating the MTR embrittlement data with fast neutron fluence (Φ) for E > 1.0 MeV resulted in an underestimation of ΔNDTT for supports in the cavity.

Several studies pertaining to radiation damage of PWR vessel supports [3-6] were conducted between 1978 and 1987. During this period, apparently there was no reason to believe that low-temperature (<100°C) MTR embrittlement data, correlated with displacements per atom (dpa) for E > 0.1 MeV, were not appropriate for evaluating embrittlement of PWR vessel supports. However, late in 1986, data from the High Flux Isotope Reactor (HFIR) [7] vessel surveillance program [8,9] indicated that the embrittlement rates of the several HFIR vessel materials (A212-B, A350-LF3, A105-II) were substantially greater than anticipated on the basis of MTR data [9]. Further evaluation of the HFIR data suggested that a fluence-rate effect was responsible for the apparent discrepancy, and shortly thereafter it became apparent that this rate effect was applicable to the evaluation of LWR vessel supports. As a result, the Nuclear Regulatory Commission (NRC) requested that the Oak Ridge National Laboratory (ORNL) evaluate the impact of the apparent embrittlement rate effect on the integrity of light-water-reactor (LWR) vessel supports. Of course, the concern over radiation embrittlement is that it increases the potential for propagation of flaws, and this could lead to the failure of the supports.

The purpose of the study was to provide an indication of whether the integrity of reactor vessel supports is likely to be challenged by radiation-induced embrittlement before 32 EFPY. The scope of the evaluation included

1. correlation of the HFIR data for application to the evaluation of LWR vessel supports,
2. a survey and cursory evaluation of all U.S. LWR vessel support designs,
3. selection of two plants for specific-plant evaluation, and
4. a specific-plant evaluation of both plants to determine critical flaw sizes for their vessel supports.

This paper discusses items 1 and 2 and the specific-plant evaluation for one of the two plants selected in item 3.

HFIR VESSEL SURVEILLANCE DATA

HFIR [7] is a high-performance, light-water-cooled, low-temperature (50 to 70°C), research reactor at ORNL that began operation in 1965. Its stainless-steel-clad, carbon-steel, pressure vessel was designed for 20 EFPY, and a surveillance program was maintained to monitor the actual radiation-induced embrittlement [8]. Late in 1986, a reevaluation of the integrity of the vessel was commenced in an effort to extend the permissible life [9]. The surveillance data indicated that the embrittlement rate was significantly greater than had been anticipated on the basis of data obtained in the early 1960s from MTRs [1]. The neutron energy spectra and the irradiation temperatures for the HFIR surveillance specimens and for MTR specimens were believed to be essentially the same, and the materials were similar; however, the fast neutron flux (ϕ) in the MTRs was ~10^5 times that in the HFIR specimens. Thus, it appeared that the lower flux in HFIR was responsible for the relatively large amount of embrittlement per neutron; that is, there appeared to be a negative fluence-rate effect.

HFIR vessel shell material (A212-B) and beam-tube nozzle materials (A105-II and A350-LF3) were included in the HFIR vessel materials surveillance program. Surveillance specimens of A212-B were removed for testing after 15.0 and 17.5 EFPY, and A105-II and A350-LF3 specimens were removed after 2.3, 6.5, 15.0, and

17.5 EFPY. The corresponding ΔNDTT data [10] are compared in Fig. 2 [ΔNDTT vs Φ (E > 1.0 MeV)] with the MTR data [1] available at the time the vessel was designed. If it is assumed that spectrum and chemistry effects are not responsible for the incongruity of the several sets of data, the comparison indicates a fluence-rate effect.

To evaluate the effects of possible differences in chemistry and fast spectrum, HFIR archive A212-B material was recently irradiated in the Oak Ridge Research Reactor (ORR), a typical high-flux, low-temperature MTR, and the HFIR and ORR A212-B data were plotted as a function of dpa for E > 0.1 MeV (Fig. 3)

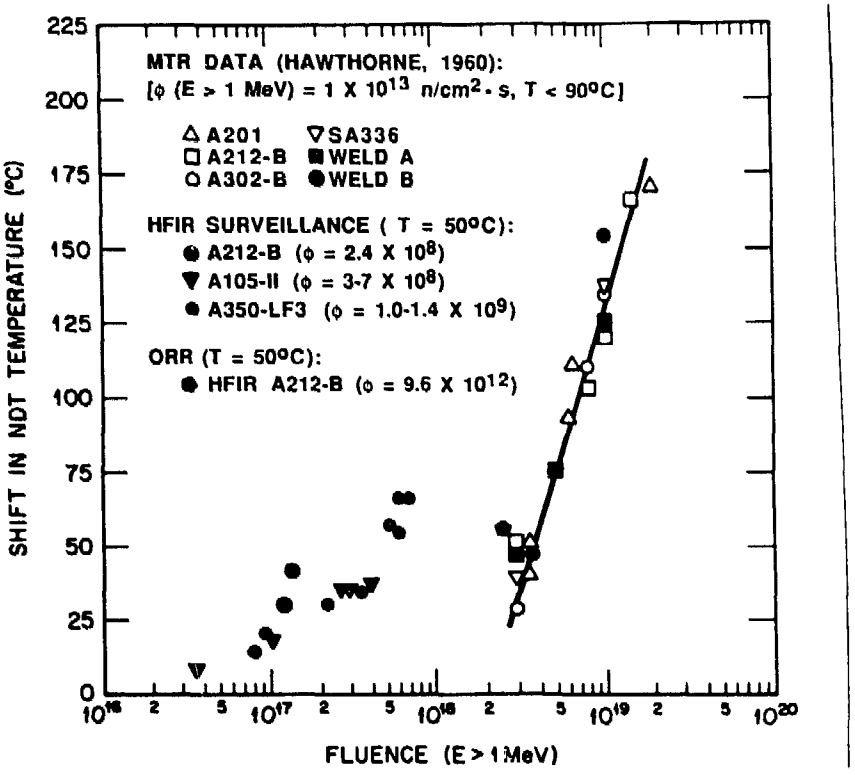

Fig. 2. Increase in NDTT with fast neutron fluence for irradition in HFIR (surveillance positions), ORR and MTR (Hawthorne, 1960).

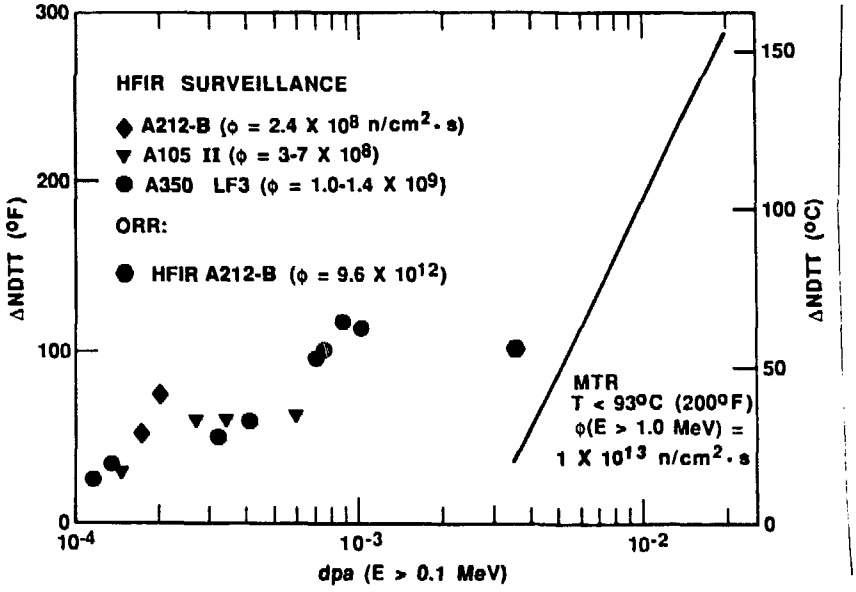

Fig. 3. Increase in NDTT with dpa for irradiations in HFIR (vessel surveillance positions), ORR, and MTR (Hawthorne, 1960).

as well as a function of Φ for E > 1.0 MeV (Fig. 2). Figure 2 shows the A212-B archive material (irradiated in the ORR) to be consistent with the MTR data, implying that the chemistry of the HFIR A212-B material is not significantly different from that corresponding to the MTR data (assuming that a difference in spectrum does not compensate for a difference in chemistry). Figure 3 shows that when the HFIR and MTR data are plotted as a function of dpa (E > 0.1 MeV), there is still evidence of a significant rate effect. Thus, the small differences in the HFIR and MTR fast spectra are not responsible for the incongruity in Fig. 2.

In the above discussion of a rate effect, only neutron energies $\geq$ 0.1 MeV were considered. Nanstad et. al., [11] and Mansur and Farrell [12] have suggested that lower energies, particularly thermal, may at least in part explain the relatively high embrittlement rates in HFIR. This possibility is being explored but was not considered in this study.

APPLICATION OF HFIR DATA TO VESSEL SUPPORT EVALUATION

The indicated embrittlement rate effect presumably applies to the supports of some LWR vessels because fast neutron fluxes, irradiation temperatures, and materials appear to be similar to those in HFIR. Temperatures of the supports range from ~250°C at the point of contact with the vessel to <65°C at a point of contact with the biological shield (65°C is the normal maximum permissible operating temperature of the concrete biological shield). The temperature of the HFIR vessel and surveillance specimens is ~50°C. Thus, presumably a portion of the support operates at a temperature close to that of the HFIR vessel.

Multigroup neutron transport calculations were performed recently for the vessel wall and the cavity of one boiling-water reactor (BWR) and three PWRs [13,14], and Table 1 summarizes the fast fluxes (E > 1.0 MeV) [as well as dpa rate (E > 0.1 MeV)] for the LWR cavities and the HFIR surveillance specimens. It is apparent that ϕ (E > 1.0 MeV) values for the PWR cavities are similar to those for the HFIR surveillance specimens (10^8 to 10^9 neutrons/cm^2·s), while that for the BWR is much less.

Table 2 summarizes LWR fast-flux data for E > 1.0 MeV (group A) and 0.1 $\leq$ E $\leq$ 1.0 MeV (group B). These data indicate that the ratio of group A to group B fluxes is much less in the cavity than it is at the inner surface of the vessel wall (the result of inelastic scattering in the vessel wall). Thus, the fast flux (E > 0.1 MeV) in the LWR cavity is much softer than that at the location of the HFIR surveillance specimens. As suggested in the last section, to account for this difference in energy spectrum when applying the HFIR data to the evaluation of the supports in the cavity, the ΔNDTT data can be correlated

Table 1. Summary of fast neutron fluxes (E > 0.1 MeV)for cavities of "typical" LWR's and for HFIR surveillance specimens

Reactor[a]	ϕ(E > 1.0 MeV) (neutrons/cm^2·s)	dpa rate (E > 0.1 MeV) (s^{-1})
HFIR	2.4×10^8—1.4×10^9	3.7×10^{-13}—2.0×10^{-12}
GE (BWR)	2.8×10^7	6.3×10^{-14}
B&W (PWR)	2.1×10^8	6.8×10^{-13}
W (PWR)	6.1×10^8	4.7×10^{-12}
CE (PWR)	1.8×10^9	5.0×10^{-12}

[a]Reactor designers: General Electric (GE), Babcock and Wilcox (B&W), Westinghouse (W),and Combustion Engineering (CE)

Table 2. Comparison of vessel and cavity calculated fluxes for "typical"BWR and PWR plants

Reactor	Neutron flux (neutrons/cm^2·s)					
	Vessel inner surface			Cavity		
	A[a]	B[a]	A/B	A	B	A/B
GE (BWR)	6.3×10^8	3.5×10^8	1.8	2.8×10^7	1.1×10^8	0.3
B&W (PWR)	5.8×10^9	7.4×10^9	0.8	2.1×10^8	1.6×10^9	0.1
W (PWR)	2.6×10^{10}	2.7×10^{10}	1.0	6.1×10^8	1.3×10^{10}	0.5
CE (PWR)	4.6×10^{10}	5.6×10^{10}	0.8	1.8×10^9	1.0×10^{10}	0.2

[a] A: $E > 1.0$ MeV
B: $0.1 \leq E \leq 1.0$ MeV

with dpa rate and dpa for $E > 0.1$ MeV instead of ϕ and Φ for $E > 1.0$ MeV, the assumption being made that most of the neutrons contributing to embrittlement have energies >0.1 MeV. A comparison of dpa rate ($E > 0.1$ MeV) for HFIR and the LWR cavities (Table 3) indicates that the maximum cavity dpa rate (5.0×10^{-12} s^{-1}) is about twice the maximum HFIR dpa rate (2.0×10^{-12} s^{-1}), while the maximum fast-flux values ($E > 1.0$ MeV) are about the same. This result indicates that some extrapolation of the HFIR data is necessary.

Application of the HFIR data to the LWR vessel supports requires extrapolation with regard to both dpa rate and dpa. Thus, correlations between ΔNDTT,

Table 3. Summary of calculated critical flaw depths for Trojan

Location on beam	Loading condition[a]	Flaw type	Critical flaw depth, a (mm)					
			7.48 EFPY[b]		32 EFPY			
			a/ℓ[c]		a/ℓ			
			0	0.1	0	0.1	0.2	0.3
Shield inner surface	A	Surface semi-ellipse	29	>32	21	>32		
	B		27	>32	20	32	>32	
	C		23	>32	17	25	>32	
Maximum bending moment	A	Surface semi-ellipse	29	>32	19	30	>32	
	B		27	>32	18	26	>32	
	C		22	>32	15	20	28	>32
Flange grout hole	A	Twin edge cracks	>50		41			
	B		>50		30			
	C		>50		11			

[a] A = DW + T + OBE, B = DW + T + SSE, and C = DW + T + SBLOCA.

[b] Corresponds to late 1988.

[c] Ratio of maximum depth (a) to surface length (ℓ).

dpa rate, and dpa are required. A proposed correlation between ΔNDTT and dpa is shown in Fig. 4. The correlation was obtained by first plotting the HFIR A350-LF3 data on log-log paper and constructing a best-fit, straight-line curve. Next, the ORR A212-B data obtained in connection with the recent HFIR vessel study [9] and a much earlier study [15] of the vessel for the experimental gas-cooled reactor (EGCR) at ORNL were plotted, and a straight line was constructed. Finally, the MTR data [1] above ΔNDTT = 40°C were plotted and a straight line was constructed. The indication is that the relatively high fast-flux data (ORR and MTR) are essentially parallel to the HFIR A350-LF3 data. This was used as justification for constructing a curve through the HFIR A212-B data points (upper curve) parallel to the A350-LF3 curve. The upper A212-B point was used as a conservative measure.

One might argue that the small difference in fast fluxes corresponding to the HFIR A212-B and A350-LF3 irradiations (2.4×10^8 and 1.2×10^9 neutrons/$cm^2 \cdot s$) relative to the factor of $\sim 10^5$ between HFIR and the MTRs ($\sim 10^8$ and 10^{13} neutrons/$cm^2 \cdot s$) would not permit distinguishing between the two HFIR fluxes with regard to establishing a rate effect. However, Hamilton [16] recently presented data indicating that, for an irradiation temperature at 100°C, there was essentially no rate effect in the fast flux (E > 1.0 MeV) range of 1×10^{10} to 3×10^{13} neutrons/$cm^2 \cdot s$. This finding indicates that the ΔNDTT differences observed between HFIR and the MTRs are associated with a rate effect below a fluence rate of $\sim 1 \times 10^{10}$ neutrons/$cm^2 \cdot s$. Thus, for this study, the observed differences in ΔNDTT for fluxes of 2.4×10^8 and 1.2×10^9 neutrons/$cm^2 \cdot s$ were considered to be real. There is, however, an inconsistency with regard to the A105-II data: although these data correspond to an intermediate flux level ($3–7 \times 10^8$ neutrons/$cm^2 \cdot s$), they tend to coincide with the A350-LF3 data, which correspond to a higher flux (1.2×10^9 neutrons/ $cm^2 \cdot s$). Perhaps this implies that a rate effect is not discernible within the flux range of 2.4×10^8 to 1.2×10^9 neutrons/$cm^2 \cdot s$. However, for this study, the A105-II data were discounted insofar as establishing a rate effect.

The second correlation for extrapolation and interpolation of the HFIR data was obtained by assuming dpa α (dpa rate)$^{\eta}$ for a given value of ΔNDTT. Corresponding values of dpa, dpa rate, and ΔNDTT were taken from Fig. 4 to obtain the log-log plot in Fig. 5.

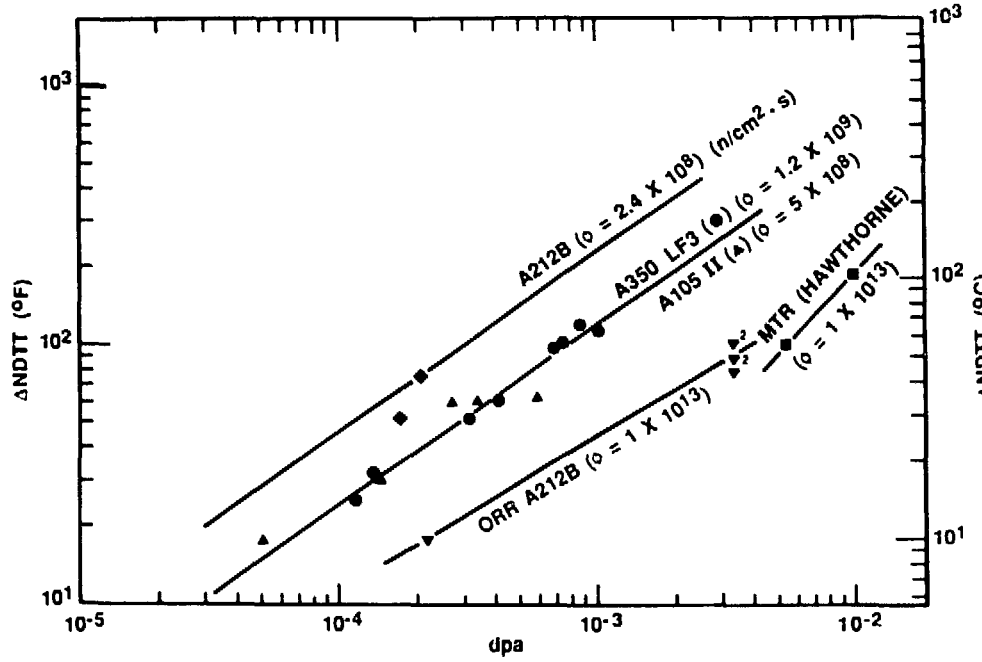

Fig. 4. Method for extrapolating HFIR vessel surveillance ΔNDTT vs dpa (E > 0.1 MeV) data, assuming $\Delta NDTT \propto dpa^{0.688}$ for $10 \leq \Delta NDTT \leq 150$°C.

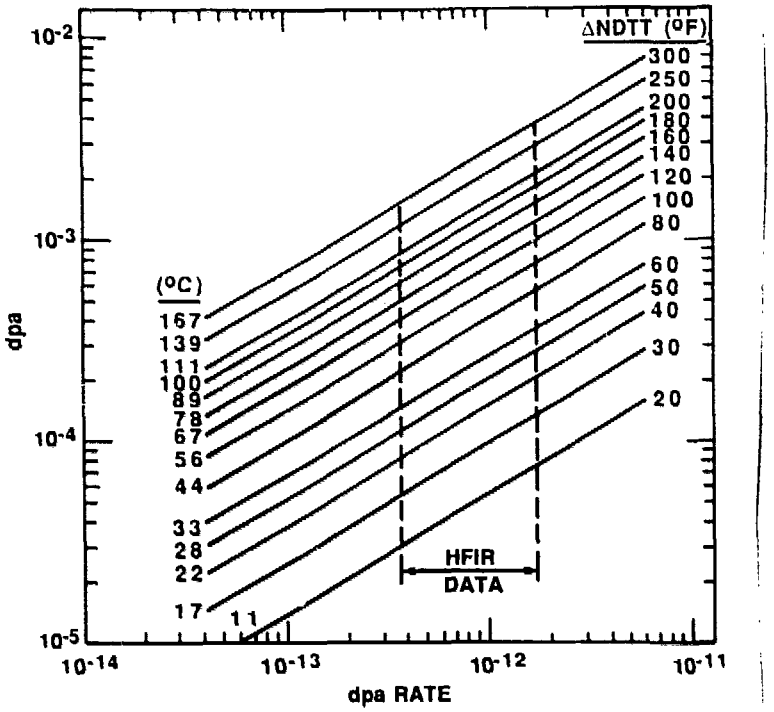

Fig. 5. dpa (E > 0.1 MeV) vs dpa rate for specific values of ΔNDTT.

SELECTION OF LWR PLANTS FOR SPECIFIC-PLANT ANALYSIS

A survey and cursory evaluation was made of all LWR vessel supports using final safety analysis reports (FSARs) and information provided in two previous related studies by Hopkins [5] and Knorovski et al. [3]. This information was then used in the selection of two LWR plants that would be subjected to specific-plant evaluation of the impact of radiation-induced embrittlement on the integrity of the reactor vessel supports. Criteria established for selection of the two plants follow.

The plants should be among those having a relatively high potential for failure of vessel supports as a result of radiation-enhanced propagation of flaws. Compliance with this condition was judged on the basis of the following considerations:

1. A potentially critical portion of the support should be exposed to the relatively high-neutron-flux regions of the cavity (from midheight to the end of the core).
2. The support material should have a relatively high potential for radiation embrittlement.
3. The portion of the support within the high-flux region should be subjected to relatively high tensile stress. Primary-load tensile stresses are of particular concern, but secondary tensile stresses (thermal and residual) can also have a significant effect.
4. The potentially critical portion of the support should have a relatively high potential for flaws of critical size.

Information in Table 1 indicates that the cavity fluxes for the BWRs are much less than those for PWRs, and BWR vessels are supported on skirts that are far removed from the bottom end of the core. (Big Rock Point is an exception but was not considered because of its uniqueness.) Thus, BWRs were excluded from consideration. All but one of the B&W PWRs are supported on skirts, and they also were excluded from consideration.

About 10% of the PWR vessels are supported on long columns and another 10% on shield tanks that extend the length of the core and thus are exposed to the

maximum fluence. At the outset of this study the PWR vendors and the Electric Power Research Institute (EPRI) were contacted informally and given the opportunity to contribute to the study. CE and EPRI responded (informally) with updated analyses of the long columns (CE) and shield tanks (EPRI, Stone and Webster), considering the HFIR surveillance data. The preliminary indication was that critical flaw sizes corresponding to 32 EFPY were "acceptably" large. Thus, these supports also were excluded from consideration in this study.

The remaining PWR vessel supports fall in a category referred to as "short column" that includes, as one extreme, very short, stubby supports (columns) that rest directly on the concrete biological shield at an elevation above the upper end of the core, where the flux is relatively low; the other extreme includes columns that extend to about midheight of the core and rest on steel cantilever beams. Only Trojan and perhaps Davis Besse are of this latter type, while Turkey Point Units 3 and 4 (identical supports) are similar to Trojan but with the steel cantilever beams located closer to the top of the core, where the flux is somewhat less. It appeared that of all those plants in the short-column category, Trojan and Turkey Point have the greatest potential for fracture-related failure of the vessel supports. Thus, they were selected for the two specific-plant analyses. Both designs include cantilever beams in high-flux regions of the cavity, and both cantilevers are stressed in tension by primary loads. Because Trojan appears to have the greatest potential of the two and because of space limitations in this paper, only the Trojan evaluation is discussed herein.

EVALUATION OF VESSEL SUPPORTS FOR TROJAN

Scope

The scope of the specific-plant evaluation consisted of (1) acquisition of design and operating data, including loads and loading rates, from the utilities; (2) a detailed stress analysis of the beam; (3) a determination of fracture properties based on published data and HFIR surveillance data; and (4) a parametric fracture analysis to determine a range of critical flaw sizes.

Support Design

The Trojan vessel is supported at four main coolant-line nozzle locations. Each support structure is comprised of an upper component (shear frame) that resists horizontal loads, a lower component (two cantilever beams) that resists vertical loads, and two pinned columns that transfer vertical loads from a vessel nozzle to the lower component, which is located at an elevation just below midheight of the core (Fig. 6). The cantilever beams extend radially from the cavity into the concrete biological shield, where they are attached to two steel pedestals that are also embedded in the concrete (Figs. 6 and 7). The beam is a double-webbed weldment, and the material is A36, a commonly used bridge steel. The beam is believed to be the critical component of the support and is the only component that was subjected to a detailed evaluation. An unusual feature in the Trojan beam is a 100-mm-diam grout hole in the top and bottom flanges directly above the pedestals (Fig. 7). The holes were flame cut, introducing the possibility of quench cracks, a localized reduction in fracture toughness and residual stresses.

Loads

All loads and loading rates applied to the vessel supports were supplied by the utilities. Individual loads include the vessel deadweight and contents (DW), thermal loads resulting from differential expansion (T), the operating basis earthquake (OBE), the safe shutdown earthquake (SSE), and a small-break loss-of-coolant accident (SBLOCA). A suitable maximum credible load for this study was

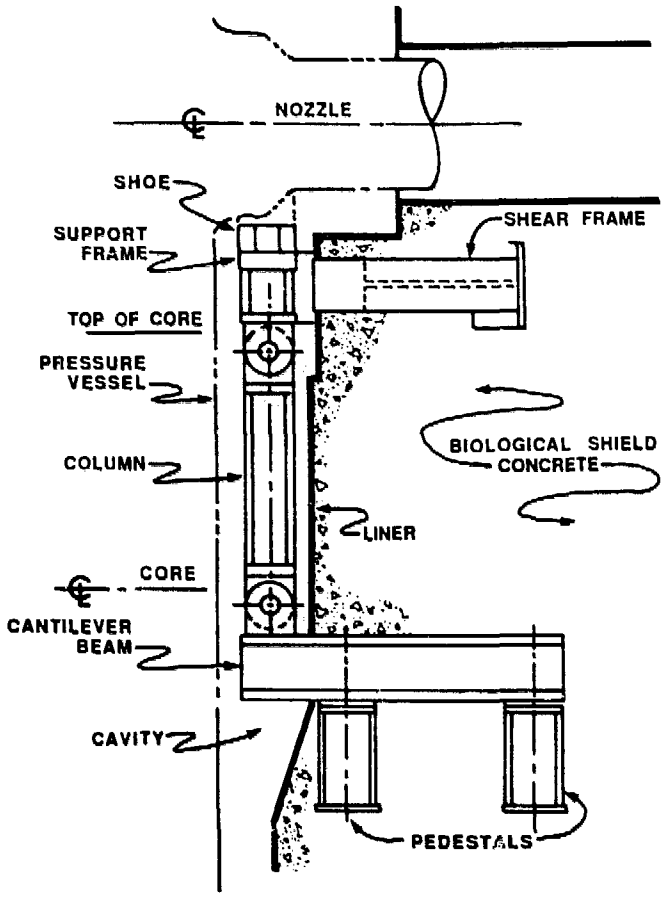

Fig. 6. Vessel support for Trojan.

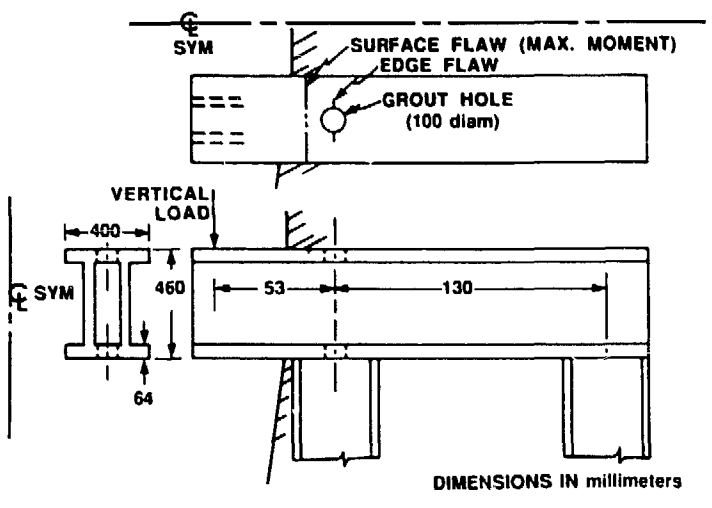

Fig. 7. Details of Trojan cantilever beam.

specified by the utility as DW + T + SBLOCA. The SBLOCA was a bounding case involving failure of auxiliary coolant lines.

The rate of loading was included because the fracture toughness of the beam material is load-rate sensitive.

Temperature

Operating temperatures of the supports for Trojan range from ~250°C at the point of contact with the nozzles to <65°C at the biological shield. The temperature of the cantilever beam was estimated to be ~32°C.

Neutron Fluxes

The neutron fluxes and dpa rates used in this study were obtained from multigroup transport calculations performed by the reactor designer (Westinghouse). Actual and postulated future changes in the fuel-loading schemes to reduce fast-neutron leakage were considered.

Material Properties

The material properties of primary concern for the cantilever beams are the fracture toughness, the initial value of NDTT, and the increase in NDTT as a function of dpa. A few dynamic fracture-toughness data (K_{Id}) are available for the beam material (A36), and they span the appropriate strain rate for the beam, thus permitting interpolation [17]. Corrections were made to the interpolated curve for lack of plane strain in the beam, where appropriate, in accordance with Ref. 18. A lower-bound curve was constructed by shifting the modified interpolated curve by ~28°C, consistent with the assumption that at T = NDTT + 17°C, K_{Id} is high enough to preclude cleavage fracture [19].

Initial values of NDTT were not available for the specific heats of material used for the beams. A best-estimate value of -2°C was obtained from Ref. 17. The radiation-induced increase in NDTT was assumed to be in accordance with the trends provided in Fig. 5.

Stress and Fracture Analyses

The potential for propagation of flaws was evaluated using linear-elastic fracture mechanics, which requires knowledge of the stresses in the structure and the fracture toughness of the material. The output of the fracture-mechanics analysis for this study is the critical flaw size, that is, the size of the smallest flaw that will propagate under a given set of assumed conditions and result in failure of the support. If the critical flaw size is small enough that the critical flaw is likely to exist, then the frequency of failure is equal to the frequency of application of the assumed load.

Because the cantilever beam rests on pedestals and the pedestals and a portion of the beam are embedded in concrete, a beam-on-elastic-foundation type of stress analysis was appropriate. Calculations of this type were made with and without the concrete between the shield liner and the inner face of the inboard pedestal because of concerns that this section of concrete would not carry load as a result of not actually being in contact with the underside of the beam. Calculations were also made with and without the reinforcing steel present. Results of these calculations indicate that the reinforcing steel has a negligible effect and that removal of the innermost section of concrete increases the maximum bending moment by 15% and the moment at the grout hole by 21% (Fig. 8).

The critical part of the beam is the upper flange because that is the location of the maximum nominal tensile stresses. Stress-intensity factors (K_I) for flaws in the flange were calculated assuming the flange to be a detached finite-width plate.

With regard to critical locations along the length of the beam (flange), it was necessary to consider (1) the compensating effects of increasing stress [up to the point of maximum bending moment (Fig. 8)] and decreasing fluence; and (2) the stress concentration introduced by the grout hole. As a result, several assumed flaw locations and shapes were included in the fracture analysis.

Semielliptical surface flaws were considered at locations along the length of the beam corresponding to the inner surface of the shield and the maximum moment, while through-thickness edge cracks were considered in the grout hole (Fig. 7).

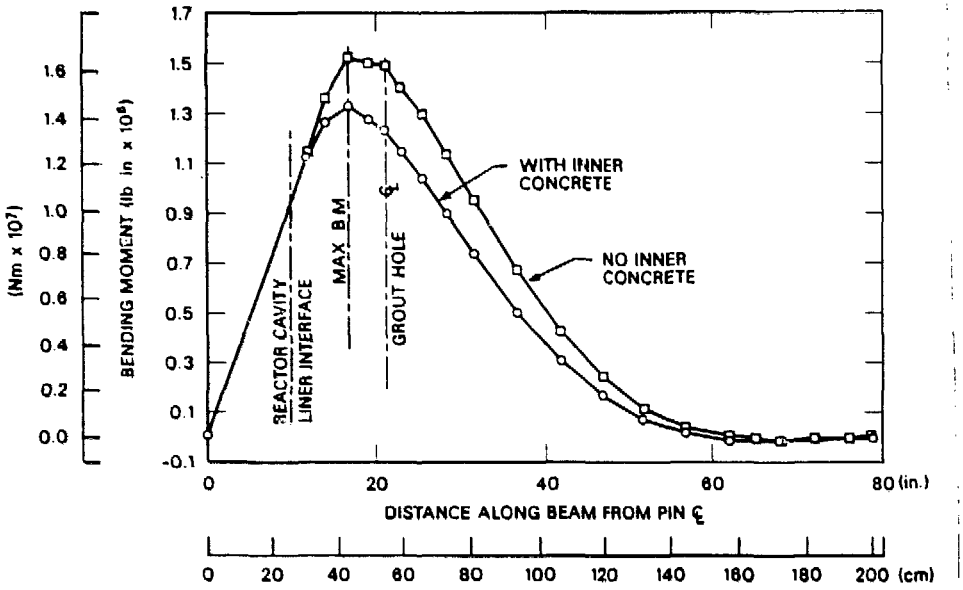

Fig. 8. Bending moment in Trojan reactor vessel support beam produced by a 100-kip (445-kN) load.

Results

Calculated critical flaw sizes are given in Table 3 consistent with no residual stress and no inner concrete. Values are listed for each loading condition considered, for operating times corresponding to the present (late 1988) and 32 EFPY, and for the different locations on the cantilever beam upper flange. At 32 EFPY the minimum critical flaw size (11 × 64 mm) is small enough to be of concern.

For deeper cracks than those included in Table 3, the stress-intensity factors are greater. Thus, crack initiation (onset of propagation) results in failure of the beam; that is, crack arrest does not take place as long as the load is applied.

Residual stresses are likely to exist in the beams, particularly around the grout hole. To obtain some indication of the sensitivity of critical flaw size to residual stress around the grout hole, it was assumed that the bending stress plus the residual stress was equal to the yield stress. For this condition, the 32-EFPY critical flaw size was reduced by ~50%.

An estimation of the probability of the existence of flaws was not included in the scope of this study. However, an analysis was conducted that indicates no significant fatigue growth of flaws in the beams during the 32-EFPY period. Thus, if corrosion is not a viable mechanism for flaw growth, the flaws included in Table 3 would have existed at the time of construction, at which time they might have been detected by a careful inspection.

CONCLUSIONS

1. The calculated minimum critical flaw sizes are small enough to be of concern.
2. Inspection for flaws at the critical locations probably is not possible because that portion of the beam is embedded in concrete.
3. The probability that the critical flaw sizes are smaller than indicated is fairly high because the values in Table 3 are best-estimate values assuming no residual stresses, and the uncertainty in several input parmeters (radiation-damage trend curve, fracture toughness, operating temperature, and loading conditions) is large.
4. Low-cycle fatigue is not a mechanism for creating flaws of critical size.

REFERENCES

1. Hawthorne, J. R., *Studies of Radiation Effects and Recovery of Notch Ductility of Pressure Vessel Steels*, British Nuclear Energy Conference, Iron and Steel Institute, London, England, November 30, 1960.
2. Steele, L. E., et al., *Irradiated Materials Evaluation and Reactor Pressure Vessel Surveillance for the Army Nuclear Power Program*, NRL Memorandum Report 1644, September 1, 1965.
3. Knorovski, G. A., Krieg, R. D., and Allen, Jr., G. C., *Fracture Toughness of PWR Components Supports*, NUREG/CR-3009 (SAND78-2347), Sandia National Laboratory, February 1983.
4. *Requirements and Guidelines for Evaluating Component Support Materials Under Unresolved Safety Issue A-12*, EPRI NP-3528, Electric Power Research Institute, June 1984.
5. Hopkins, W. G., and Grove, W. L., *A Study of the Embrittlement of Reactor Vessel Steel Supports, Reactor Dosimetry*, Vol. 2, ed., J. P. Genthon and H. Rottger, Dordrecht, Netherlands: D. Reidel Publishing Company, 1985, pp. 621–28.
6. Hopkins, W. G., *Reactor Pressure Vessel Supports for Pressurized Water Reactors and Boiling Water Reactors, Residual Life Assessment of Major Light Water Reactor Components — Overview, Volume 1*, NUREG/CR-4731 (EGG-2469), Vol. 1, Idaho National Engineering Laboratory, June 1987.
7. Cheverton, R. D., and Sims, T. M., *HFIR Core Nuclear Design*, ORNL-4621, Union Carbide Corp. Nucl. Div., Oak Ridge Natl. Lab., July 1971.
8. McWherter, J. R., Schappel, R. E., and McGuffey, J. R., *HFIR Pressure Vessel and Structural Components Material Surveillance Program*, ORNL/TM-1372, Union Carbide Corp. Nucl. Div., Oak Ridge Natl. Lab., January 1966.
9. Cheverton, R. D., Merkle, J. G., and Nanstad, R. K., eds., *Evaluation of HFIR Pressure-Vessel Integrity Considering Radiation Embrittlement*, ORNL/TM-10444, Martin Marietta Energy Systems, Inc., Oak Ridge Natl. Lab., April 1988.
10. Nanstad, R. K., et al., *Effects of 50 C Surveillance and Test Reactor Irradiation on Ferritic Pressure Vessel Steel Embrittlement*, presented at 14th International Symposium on the Effects of Radiation on Materials, Andover, Massachusetts, June 27, 1988 (to be published in ASTM STP).
11. Nanstad, R. K., et al., "Accelerated Neutron Embrittlement of Ferritic Steels at Low Fluence: Flux and Spectrum Effects," *J. of Nuc. Matls.* 158, 1–6 (1988).
12. Mansur, L. K., and Farrell, N. K., private communication to Cheverton, R. D., and Nanstad, R. K., September 1988.
13. Tsoulfanidis, N., et al., "Neutron Energy Spectrum Calculations in Three PWR's," pp. 693–701 in *Proceedings of the Fifth ASTM-EURATOMS Symposium on Reactor Dosimetry* (1985).
14. Williams, M. L., Oak Ridge Natl. Lab., personal communication to Kam, F., Oak Ridge Natl. Lab.
15. Wechsler, M. S., et al., *Radiation Hardening and Embrittlement in a Low-Carbon Pressure Vessel Steel, Irradiation Effects in Structural Alloys for Thermal and Fast Reactors*, STP 457, pp. 242–60, American Society for Testing and Material, Philadelphia, 1969.
16. Hamilton, M. L., and Heinesch, H. L., "Tensile Properties of Neutron Irradiated A212-B Pressure Vessel Material," ASTM 14th International Symposium on Effects of Radiation on Materials, Andover, Massachusetts, June 27–29, 1988.
17. *Structural Alloys Handbook*, 1987 ed., Vol. 3, Battelle Columbus Laboratory, Columbus, Ohio.
18. Rolfe, S. T., and Barsom, J. M., *Fracture and Fatigue Control in Structures: Applications of Fracture Mechanics*, Prentice Hall, Inc., Englewood Cliffs, New Jersey, 1977.
19. *The American Society of Mechanical Engineers Boiler and Pressure Vessel Code*, Sect. III, Subsect. NF.